Table 1. Summary of crystallographic information.

	Free enzyme	CoA complex
Space group	*C*2	$P2_1$
Maximum resolution (Å)	2.7	2.7
Number of observations	533,916	168,936
R_{merge} (%)*	7.6 (18.1)	5.2 (11.6)
Resolution range for refinement	30–2.7 Å	30–2.7 Å
Number of reflections	113,103	59,546
Completeness (%)	94.5	93.2
R factor (%)†	22.6 (29.9)	22.6 (29.6)
Free *R* factor (%)	26.2 (34.8)	27.9 (33.4)
rms deviation in bond lengths (Å)	0.009	0.009
rms deviation in bond angles (°)	1.4	1.4

*$R_{merge} = \sum_h \sum_i |I_{hi} - \langle I_h \rangle| / \sum_h \sum_i I_{hi}$. The numbers in parentheses are for the highest resolution shell. †$R = \sum_h |F^o_h - F^c_{dh}| / \sum_h F^o_h$.

(Fig. 3A). Leu[1705] is unlikely to contact the substrate directly as it is about 8 Å from the thiol group of CoA (Fig. 3A). Thus, mutagenesis and structural information suggest that the herbicides target the active site of CT.

Our kinetic experiments showed that the herbicide haloxyfop is a competitive inhibitor of yeast CT with respect to the substrate malonyl-CoA (Fig. 3C), which is consistent with herbicide binding at the active site. The inhibition of yeast CT by haloxyfop is very weak, with an inhibition constant (K_i) of about 0.5 mM (Fig. 3C). The herbicide is a poor inhibitor of the L1705I mutant of yeast CT as well (table S1)(*19*). These observations, together with those on the apicoplast ACC of *Toxoplasma gondii* (*21*), indicate that there are additional structural determinants for the binding of these compounds to the active site of CT.

Based on the structural, biochemical, and mutagenesis observations, it may be possible that part of the herbicide is bound in the cavity between the two domains in the active site (Fig. 3A). This cavity extends from the thiol group of CoA to the side chains of Leu[1705] and Ser[1708] and is mostly hydrophobic in nature. The proximity of the inhibitor to Leu[1705] is consistent with its importance in determining the herbicide sensitivity of plant ACCs. The carboxyl group of the inhibitor may mimic the carboxyl group in the malonyl-CoA substrate of the enzyme.

The successful development of inhibitors against the active site of the CT domain of plant ACCs holds promise for the development of inhibitors against other CT domains, especially that of human ACC2. The control of herbicide sensitivity by a single amino acid in the wheat enzyme demonstrates that it could also be possible to identify highly selective inhibitors of mammalian enzymes. For example, inhibitors that target human ACC2 while having only minor effects on ACC1 may prove beneficial for controlling body weight (*8*). Our structural information about the CT domain provides a starting point for understanding the catalysis by this enzyme as well as for designing and optimizing its inhibitors.

References and Notes

1. A. W. Alberts, P. R. Vagelos, in *The Enzymes*, P. D. Boyer, Ed. (Academic Press, New York, 1972), vol. 6, pp. 37–82.
2. S. J. Wakil, J. K. Stoops, V. C. Joshi, *Annu. Rev. Biochem.* **52**, 537 (1983).
3. J. R. Knowles, *Annu. Rev. Biochem.* **58**, 195 (1989).
4. J. E. Cronan Jr., G. L. Waldrop, *Prog. Lipid Res.* **41**, 407 (2002).
5. J. D. McGarry, N. F. Brown, *Eur. J. Biochem.* **244**, 1 (1997).
6. R. R. Ramsay, R. D. Gandour, F. R. van der Leij, *Biochim. Biophys. Acta* **1546**, 21 (2001).
7. J. W. Campbell, J. E. Cronan Jr., *Annu. Rev. Microbiol.* **55**, 305 (2001).
8. L. Abu-Elheiga, M. M. Matzuk, K. A. H. Abo-Hashema, S. J. Wakil, *Science* **291**, 2613 (2001).
9. J. M. Lenhard, W. K. Gottschalk, *Adv. Drug Delivery Rev.* **54**, 1199 (2002).
10. K. L. Levert, G. L. Waldrop, J. M. Stephens, *J. Biol. Chem.* **277**, 16347 (2002).
11. O. Zagnitko, J. Jelenska, G. Tevzadze, R. Haselkorn, P. Gornicki, *Proc. Natl. Acad. Sci. U.S.A.* **98**, 6617 (2001).
12. W. A. Hendrickson, *Science* **254**, 51 (1991).
13. S. E. Polakis, R. B. Guchhait, E. E. Zwergel, M. D. Lane, *J. Biol. Chem.* **249**, 6657 (1974).
14. M. M. Benning *et al.*, *Biochemistry* **35**, 8103 (1996).
15. C. K. Engel, M. Mathieu, J. P. Zeelen, J. K. Hiltunen, R. K. Wierenga, *EMBO J.* **15**, 5135 (1996).
16. J. Wang, J. A. Hartling, J. M. Flanagan, *Cell* **91**, 447 (1997).
17. M. M. Benning, T. Haller, J. A. Gerlt, H. M. Holden, *Biochemistry* **39**, 4630 (2000).
18. A. M. Mursula, D. M. F. van Aalten, J. K. Hiltunen, R. K. Wierenga, *J. Mol. Biol.* **309**, 845 (2001).
19. H. Zhang, Z. Yang, Y. Shen, L. Tong, data not shown.
20. L. H. Weaver, K. Kwon, D. Beckett, B. W. Matthews, *Prot. Sci.* **10**, 2618 (2001).
21. J. Jelenska, A. Sirikhachornkit, R. Haselkorn, P. Gornicki, *J. Biol. Chem.* **277**, 23208 (2002).
22. M. Carson, *J. Mol. Graphics* **5**, 103 (1987).
23. A. Nicholls, K. A. Sharp, B. Honig, *Proteins* **11**, 281 (1991).

24. We thank R. Abramowitz and C. Ogata for setting up the X4A beamline, R. Khayat and X. Tao for help with data collection at the synchrotron, C. Frank for technical support, P. Gornicki for helpful discussions, and Columbia University (L.T.) for financial support.

Supporting Online Material

www.sciencemag.org/cgi/content/full/299/5615/2064/DC1
Materials and Methods
Figs. S1 to S4
Table S1
References

10 December 2002; accepted 24 February 2003

The Pentacovalent Phosphorus Intermediate of a Phosphoryl Transfer Reaction

Sushmita D. Lahiri,[1] Guofeng Zhang,[2] Debra Dunaway-Mariano,[2]* Karen N. Allen[1]*

Enzymes provide enormous rate enhancements, unmatched by any other type of catalyst. The stabilization of high-energy states along the reaction coordinate is the crux of the catalytic power of enzymes. We report the atomic-resolution structure of a high-energy reaction intermediate stabilized in the active site of an enzyme. Crystallization of phosphorylated β-phosphoglucomutase in the presence of the Mg(II) cofactor and either of the substrates glucose 1-phosphate or glucose 6-phosphate produced crystals of the enzyme–Mg(II)–glucose 1,6-(bis)phosphate complex, which diffracted x-rays to 1.2 and 1.4 angstroms, respectively. The structure reveals a stabilized pentacovalent phosphorane formed in the phosphoryl transfer from the C(1)O of glucose 1,6-(bis)phosphate to the nucleophilic Asp8 carboxylate.

The unique ability of enzymes to synchronize multiple interactions at specific sites with reactants, intermediates, and products defines the reaction pathway and is the source of the enormous rate acceleration accomplished by enzymes (10^7- to 10^{19}-fold) (*1–9*). The study of the reaction pathway as it proceeds within the protein walls continues to be the focal point of bioorganic chemistry. Kinetic investigations of enzyme catalysis on natural substrates and the study of unreactive mimics of the ground state and transition state have contributed greatly to our understanding of the steric and electronic structures of reaction coordinate species (*10–15*). An actual image of each chemical species formed is, however, the ultimate goal.

X-ray crystallography is the conduit to such images (*16*, *17*). If a chemical species is

long-lived within the crystalline enzyme, structure determination is possible. Indeed, structures of enzymes bound to the thermodynamically favored product are common, as are structures of enzymes bound with inhibitors modeled after the substrate or transition state. In some cases, the protonation state or structure of a catalytic residue has been altered to inhibit a specific reaction step and thus to accumulate a targeted intermediate for structure determination (*18*–*20*). In rare cases, time-resolved crystallography has been successfully used to obtain the structure of an intermediate stabilized by cryotemperature (*21*–*23*) or accumulated on the millisecond time scale after the triggering of a photolabile substrate (*24*).

Enzyme reaction intermediates can be divided into two classes: those of high intrinsic energy resulting from incomplete bonding (such as high-energy radicals, cations, and anions) or from hyperbonding (such as phosphoranes), and those of low intrinsic energy (such as carbon or phosphate esters and anhydrides, carbinolamines, imines, or enamines) (*25*). Although it has been theorized that the active site environment can stabilize enzyme-generated intermediates of high intrinsic energy, until now such species have not been accessed by x-ray crystallography. Here, we report the structure of a pentacoordinate oxyphosphorane intermediate formed in the isomerization of β-glucose 1-phosphate (G1P) to β-glucose 6-phosphate (G6P) catalyzed by β-phosphoglucomutase (β-PGM) from *Lactococcus lactis* (*26*). The hyperbonded oxyphosphorane species observed in this structure is intrinsically unstable. It has no counterpart in solution chemistry, where alkylation of the oxygen substituents is necessary for oxyphosphorane stabilization (*27*).

Phosphoglucomutases use an active-site nucleophilic residue to mediate the transfer of a phosphoryl group between the C(6)O and C(1)O positions in hexose phosphates (*28*–*33*). The active form of the mutase is phosphorylated on the nucleophilic side-chain carboxylate of Asp8 (Fig. 1). The phosphoryl group is transferred to the free hydroxyl of the hexose phosphate substrate to form the hexose 1,6-(bis)phosphate. Reorientation, followed by phosphoryl transfer from the hexose 1,6-(bis)phosphate to the enzyme catalytic group, produces the hexose phosphate product (*34*).

In this study, crystals of native and selenomethionine (SeMet)–substituted β-PGM equilibrated with Mg(II) and either G1P or G6P were grown and subjected to structural analysis (Table 1). Details of sample preparation, crystallization, and structure determination are given in (*35*). Both structures, solved at 1.2 and 1.4 Å resolution, respectively (1.7 Å for the SeMet form), revealed the enzyme–Mg(II)–glucose 1,6-(bis)phosphate (β-G1,6-P) intermediate complex (the intermediate of the first phosphoryl transfer step) (Fig. 1). The intramolecular orientation of the two protein domains comprising the β-PGM–intermediate complex makes the active-site solvent inaccessible relative to the unliganded phosphorylated enzyme-Mg(II) complex. Because the conditions used previously to crystallize the phosphorylated enzyme-Mg(II) complex (*32*) and those of the enzyme–Mg(II)–β-G1,6-P complexes in this study were identical, the possibility that the crystal environment governs the conformation can be excluded. Therefore, the conformational change (fig. S1) can be attributed to the presence of the bound ligand and the observed conformational dynamics are associated with the catalytic cycle. In addition, the nature of the crystal contacts in the β-G1,6-P intermediate complex would not be expected to differentially stabilize any one liganded form over another, although the close packing would disallow the open conformation in this crystal form. Thus, the observed intermediate is not selected by the crystal packing.

The close contacts that occur between the Mg(II) cofactor, the β-G1,6-P ligand, and the enzyme active site are pictured in Fig. 2A and are diagrammed in Fig. 2B (see also fig. S3). The most striking feature of this picture is the C(1)phosphorus. It is pentavalent, with the Asp8 OD1 and hexose C(1)O occupying apical positions, and the three P(1) oxygen atoms occupying equatorial positions of a trigonal bipyramid. The conclusion that the moiety covalently bound to the C1 position of the glucose corresponds to a phosphorus group is supported by the fact that the electron density at a high contour level covers only the Mg(II) ion, the C(6)-phosphate phosphorus, and the C(1)-phosphate phosphorus (each with a similar number of electrons). Also, no ions such as borate, nitrate, or vanadate that might mimic the pentavalent geometry were present in the purification or crystallization buffers.

The electron density in the region of the C(1) phosphorus contrasts with that in the region of the tetravalent, tetrahedral C(6) phosphorus (Fig. 2, C and D, and fig. S2A). At 1.2 Å resolution, the bond lengths and geometries of tetravalent and pentavalent phosphorus moieties can easily be distinguished, as inversion matrix calculations (*36*) of the data show that the accuracy of the bond lengths is ±0.11 Å and that of the bond angles is ±3°. In addition, because the resolution of the structure allows free-atom refinement of all ligands without geometric restraints, no model bias was imposed on the structure. The precise position of the C(1) phosphorus is defined by the electron density contoured at a high level (13σ) (Fig. 2A). The electron density at phosphorus is not elliptical, and the occupancy of all atoms in the pentavalent phosphorane is 1.0, which together indicate that the observed structure does not represent an average of the structures of the phosphorylated Asp and the phosphorylated C(1)O species. The population of any other enzyme-bound species at ≥12% would be discernable in the electron density map. The position of phosphorus was further confirmed by calculating an anomalous difference electron density map [see supporting online material text and fig. S2B]. The map gives a clear electron density peak at the C(1)P phosphorus position with density contoured at 3σ. In addition, the *B* factors of the individual atoms of the β-G1,6-P intermediate (average 9.4 Å^2) are similar to those of the main chain of the protein (average 12.0 Å^2) (see table S1 for individual atoms). The atoms corresponding to the pentavalent oxyphosphorane at C(1) have thermal motion similar to those in the tetravalent phosphate at C(6) and the glucose chain. Also, the carboxyl group of Asp8 is immobilized to a similar extent with an average *B* factor for the side chain of 9.1 Å^2.

The comparison of the bond lengths and angles of the tetravalent C(6) phosphate

[1]Department of Physiology and Biophysics, Boston University School of Medicine, Boston, MA 02118–2394, USA. [2]Department of Chemistry, University of New Mexico, Albuquerque, NM 87131, USA.

*To whom correspondence should be addressed. E-mail: allen@med-xtal.bu.edu (K.N.A.); dd39@unm.edu (D.D.-M.)

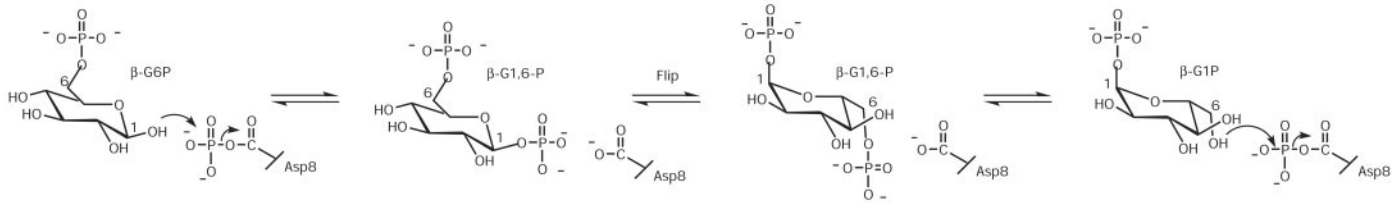

Fig. 1. The scheme for the reaction catalyzed by β-PGM. The C(1) and C(6) positions on the hexose ring are labeled.

group and the pentavalent C(1)phosphate group reveals distinct differences. The bond lengths and angles (Fig. 2, B and D) of the C(6) phosphate group observed in this structure conform to those observed in the crystal structures of phosphate monoesters (*37*). The C(1) phosphate bond lengths and bond angles (Fig. 2, B and C) more closely match those observed in the small-molecule crystal structures of the stable, fully alkylated pentavalent oxyphosphoranes [such as $(RO)_5P$] (*37*, *38*) in which the three shorter, stronger equatorial bonds assume sp^2 hybridization and the two longer, weaker apical bonds assume linear p(z)d(z2) hybridization. The lengths of the apical bonds in the enzyme-bound oxyphosphorane (calculated bond order 0.24 to 0.45) appear to be longer than those observed in the crystal structures of fully alkylated oxyphosphoranes (*39*). This difference may be ascribed to the control that the enzyme exerts over the positions of the apical substituents, one of which is the active-site aspartate and the other of which is the hexose ligand, anchored to the active site by hydrogen bonds. Overall, the results are consistent with the visualization of an intermediate species of high intrinsic energy, as it is stabilized in the active site of the enzyme.

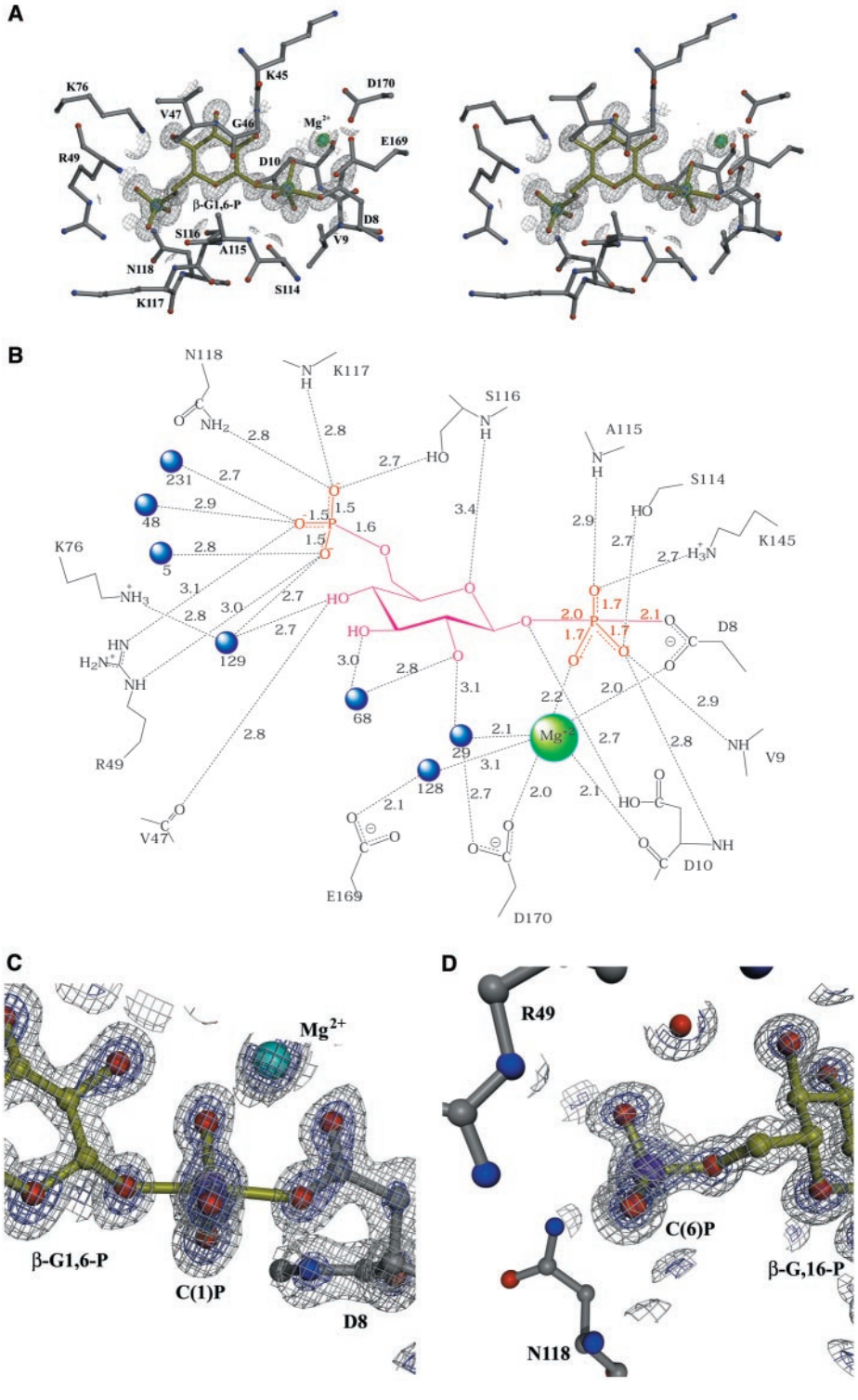

Fig. 2. The β-G1,6-P intermediate in the active site of β-PGM from the 1.2 Å resolution structure. (**A**) A stereo image in which the enzyme residues (gray) and β-G1,6-P intermediate (yellow) are shown as ball-and-stick models, with the composite-omit 2Fo-Fc electron density map contoured at 2σ (gray cages) or 13σ (green cages). (**B**) Schematic of interactions between the β-G1,6-P intermediate and β-PGM with all hydrogen bonds (<4 Å) depicted as dashed lines and labeled with bond length. Water molecules are shown as blue spheres. (**C**) View of the geometry at the pentavalent phosphorane intermediate formed between the C(1) phosphate of β-G1,6-P (yellow) and the nucleophilic Asp8 (gray) with the composite-omit 2Fo-Fc electron density map contoured at 4σ (blue cages) and 2σ (gray cages). At 1.2 Å resolution, there is no connectivity in the electron density between the apical oxygen atoms and phosphorus because the resolution is higher (1.2 Å) than the length of the apical bonds (≥2.0 Å). The bond lengths are 1.7 Å for P(1)-O^-, 2.0 Å for P-OC(1) and 2.1 Å for P-OD1 Asp8, and bond angles are 89°, 117° to 124°, and 174° versus the idealized angles of 90°, 120°, and 180° for the trigonal bipyramid. The geometry is comparable to that of pentavalent oxyphosphoranes with equatorial bond lengths of 1.57 to 1.63 Å, apical bond lengths of 1.66 to 1.76 Å, and angles of about 88° to 92°, 116° to 125°, and 176°. (**D**) View of the geometry at the C(6) phosphate of β-G1,6-P (yellow) with the composite-omit 2Fo-Fc electron density map contoured at 4σ (blue cages) and 2σ (gray cages). The bond lengths and angles are 1.5 Å for P(6)-O^- and 1.6 Å for P-OC(6), and 101° to 109°, which are comparable to those of phosphate monoesters at 1.5 and 1.6 Å; 103° to 115°.

How is the stabilization of the oxyphosphorane integral to catalysis? The backside, in-line (174° ± 3° angle) arrangement of the Asp8 OD1 nucleophile and C(1)O leaving group, conforms to the trajectory expected for the reaction coordinate of an associative nucleophilic substitution reaction at phosphorus (*40*). Although they are intrinsically unstable (*41*), ionized pentavalent oxyphosphoranes have been implicated as intermediates in both solution and enzyme-catalyzed phosphoryl transfer reactions (*38*, *40*, *42–44*). Until now, the direct observation of such an intermediate has eluded chemists. In this case, the numerous stabilizing interactions provided by the β-PGM active site shift the energetics of the phosphate ↔ oxyphosphorane equilibrium in favor of the latter. First, because the entropy is minimized in the enzyme- substrate complex [i.e., the Asp8 OD2 is anchored by Mg(II) and Lys145, and the 6-phosphoglucose moiety is immobilized by 20 hydrogen bonds (*45*)] (Fig. 2B), formation of the oxyphosphorane is not accompanied by the large entropy loss that accompanies the bimolecular solution reaction. Second, the enthalpic cost imposed by the weak apical bonds is compensated for by the formation of several strong hydrogen bonds to the two apical oxygen atoms of the trigonal-bipyramidal phosphorus (the A115 backbone NH, S114 OH, K145 ε-NH_3^+, V9 amide NH, and D10 amide NH). Using molecular modeling (*46*) to convert the trigonal-bipyramidal geometry at phosphorus to an idealized tetrahedral geometry increases the length of hydrogen bonds between the enzyme and the phosphoryl equatorial oxygens by 0.2 Å and increases the distance between the phosphorus and the Asp8 OD1 from 2.1 to 2.6 Å [too long for covalent bond formation yet close enough to be considered a "near-attack" conformation (*47*)]. Thus, the transition from the tetrahedral phosphorus of the phosphate monoester to the trigonal-bipyramidal phosphorus of the oxyphosphorane is accompanied by an increase in stabilization by the enzyme.

The equilibrium mixture generated from the incubation of the phosphorylated enzyme with G1P or the G6P is expected to consist of the phosphorylated enzyme bound to G1P or G6P in equilibrium with the unphosphorylated enzyme bound to β-G1,6-P. If stabilized reaction intermediates were to populate this mixture, they might consist of the enzyme complexes of the oxyphosphoranes resulting from the addition of G6P C(1)OH or G1P C(6)OH to the phosphorus of the aspartylphosphate group. The crystallization of the equilibrated mixture at 18°C, followed by x-ray structure determination at cryotemperature, captured the enzyme complex of one such oxyphosphorane intermediate. Thus, the image shown in Fig. 2 is unequivocal, direct visual evidence of enzyme catalysis by way of intermediate stabilization.

Table 1. Summarized data collection and refinement statistics.* MAD, multiwavelength anomalous diffraction.

Data set	SeMet MAD data sets			Native data sets	
	λ_1 (edge)	λ_2 (peak)	λ_3 (remote)	G1P	G6P
Unit cell (Å)	a = 36.93, b = 54.3, c = 104.77			a = 37.0, b = 54.3, c = 104.5	a = 37.3, b = 54.2, c = 104.4
Space group	$P2_12_12_1$			$P2_12_12_1$	
X-ray source	BNL X4A			APS 14-BMC	
Wavelength (Å)	0.97935	0.97902	0.96866	0.90000	0.90000
Resolution range (Å)	∞ – 1.7	∞ – 1.7	∞ – 1.7	∞ – 1.2	∞ – 1.4
Total/unique reflections	315,535/24,283	300,234/24,294	306,703/24,426	699,466/66,304	983,130/66,302
Completeness (%)	91.6 (64.2)	91.1 (64.7)	93.2 (69.1)	86.9 (54.4)	98.0 (88.1)
I/σ (I)	17.9 (5.5)	17.6 (5.4)	18.6 (5.6)	32.7 (12.4)	34.9 (15.7)
R_{merge}† (%)	0.069 (0.18)	0.073 (0.18)	0.064 (0.15)	0.043 (0.08)	0.073 (0.13)
f′/f″ (e^-)	–11.8/5.8	–9.5/6.2	–3.5/5.4		
Figure of merit‡ to 1.7 Å	0.4				
Solvent content	33.5%				
Number of atoms per asymmetric unit					
Protein				1744	1744
Magnesium				1	1
Bisphosphate				20	20
Water				521	402
Average B factors (Å²)					
Wilson plot				8.8	13.4
Amino acid residues				12.0	11.7
Mg^{2+} ions (1 total)				6.6	8.2
Bisphosphate				9.4	9.5
Water				15.2	14.6
Refinement statistics					
Program				SHELX§	CNS
Refinement				Anisotropic	Isotropic
Resolution (Å)				20–1.2	100–1.4
No. of reflections (working/test)				50,842/5756	37,054/4163
R_{work}‖/R_{free}¶ (%)				14.08/17.9	17.02/19.44
RMS deviations from ideal					
Bond length (Å)				0.009	0.005
Angles (degrees)				1.12	1.19
Dihedral angle				20.5	21.5
Ramachandran plot#					
Most favorable (%)				97.5	93.2
Additionally allowed (%)				2.4	6.8

*Values for the outermost shell (1.76 to 1.7 Å for SeMet, 1.22 to 1.20 Å for the G1P data set, and 1.45 to 1.40 for the G6P data set) are shown in parentheses. † $R_{merge} = \Sigma_{hkl} \Sigma_i | I_{hkl,i} - \langle I_{hkl} \rangle I | / \Sigma_{hkl} \Sigma_i | I_{hkl,i} |$, where $\langle I_{hkl} \rangle$ is the mean intensity of the multiple $I_{hkl,i}$ observations for symmetry-related reflections. ‡Reported by SOLVE. §In the final stages of refinement of the G1P structure, the program SHELXL-97 (*36*) was used to perform free-atom refinement of all ligands and anisotropic B-factor refinement with 10 cycles of conjugate gradient minimization in each stage. ‖$R_{work} = \Sigma_{hkl} |F_{obs} - F_{calc}| / \Sigma_{hkl} |F_{obs}|$. ¶$R_{free} = \Sigma_{hkl \in T} |F_{obs} - F_{calc}| / \Sigma_{hkl} |F_{obs}|$, where the test set T includes 10% of the data. #Defined by PROCHECK (*48*).

References and Notes

1. W. P. Jencks, *Adv. Enzymol. Relat. Areas Mol. Biol.* **43**, 219 (1975).
2. J. R. Knowles, *Nature* **350**, 121 (1991).
3. A. Warshel, *J. Biol. Chem.* **273**, 27035 (1998).
4. W. W. Cleland, P. A. Frey, J. A. Gerlt, *J. Biol. Chem.* **273**, 25529 (1998).
5. T. C. Bruice, S. J. Benkovic, *Biochemistry* **39**, 6267 (2000).
6. R. Wolfenden, M. J. Snider, *Acc. Chem. Res.* **34**, 938 (2001).
7. P. T. Rajagopalan, S. J. Benkovic, *Chem. Rec.* **2**, 24 (2002).
8. T. C. Bruice, *Acc. Chem. Res.* **35**, 139 (2002).
9. Q. Hu, R. Kluger, *J. Am. Chem. Soc.* **124**, 14858 (2002).
10. G. Rudnick, R. H. Abeles, *Biochemistry* **14**, 4515 (1975).
11. K. A. Johnson, *Methods Enzymol.* **249**, 38 (1995).
12. D. Dunaway-Mariano, *Methods Enzymol.* **308**, 149 (1999).
13. J. W. Gross, P. A. Frey, *Methods Enzymol.* **354**, 27 (2002).
14. W. W. Cleland, *Methods Enzymol.* **249**, 341 (1995).
15. V. L. Schramm, *Curr. Opin. Chem. Biol.* **5**, 556 (2001).
16. G. A. Petsko, D. Ringe, *Curr. Opin. Chem. Biol.* **4**, 89 (2000).

17. V. L. Schramm, W. Shi, *Curr. Opin. Struct. Biol.* **11**, 657 (2001).
18. Y. F. Li *et al., J. Biol. Chem.* **273**, 15035 (1998).
19. I. S. Ridder, H. J. Rozeboom, K. H. Kalk, B. W. Dijkstra, *J. Biol. Chem.* **274**, 30672 (1999).
20. J. Allard, P. Grochulski, J. Sygusch, *Proc. Natl. Acad. Sci. U.S.A.* **98**, 3679 (2001).
21. H. Kack, K. J. Gibson, Y. Lindqvist, G. Schneider, *Proc. Natl. Acad. Sci. U.S.A.* **95**, 5495 (1998).
22. A. Heine *et al., Science* **294**, 369 (2001).
23. I. Schlichting *et al., Science* **287**, 1615 (2000).
24. M. J. Brubaker, D. H. Dyer, B. Stoddard, D. E. Koshland Jr., *Biochemistry* **35**, 2854 (1996).
25. R. D. Allison, D. L. Purich, *Methods Enzymol.* **354**, 455 (2002).
26. N. Qian, G. A. Stanley, B. Hahn-Hagerdal, P. Radstrom, *J. Bacteriol.* **176**, 5304 (1994).
27. R. E. Hanes Jr., V. M. Lynch, E. V. Anslyn, K. N. Dalby, *Org. Lett.* **4**, 201 (2001).
28. J. B. Dai, Y. Liu, W. J. Ray Jr., M. Konno, *J. Biol. Chem.* **267**, 6322 (1992).
29. N. Qian, G. A. Stanley, A. Bunte, P. Radstrom, *Microbiology* **143 (Pt 3)**, 855 (1997).
30. L. E. Naught, P. A. Tipton, *Arch. Biochem. Biophys.* **396**, 111 (2001).
31. C. Regni, P. A. Tipton, L. J. Beamer, *Structure (Cambridge)* **10**, 269 (2002).
32. S. D. Lahiri, G. Zhang, D. Dunaway-Mariano, K. N. Allen, *Biochemistry* **41**, 8351 (2002).
33. S. Muller *et al., J. Mol. Biol.* **315**, 141 (2002).
34. In earlier work, β-PGM was isolated from the cell in its phosphorylated form and crystallized in the presence of its Mg(II) cofactor for structure determination (*32*). Overall, β-PGM is a monomer that is composed of two distinct domains: a helical cap domain and an α/β core domain. Whereas the conformations of individual domains of the phosphorylated enzyme-Mg(II) complex and the enzyme-Mg(II)-β-G1,6-P complexes are nearly indistinguishable, the positions of the cap domains relative to the core domains are noticeably different. A hinge-like motion between the two domains, acting as rigid bodies, produces the conversion of one enzyme conformer to the other, enveloping the β-G1,6-P intermediate.
35. Materials and methods are available as supporting material on *Science* Online.
36. G. M. Sheldrick, T. R. Schneider, *Methods Enzymol.* **277B**, 319 (1997).
37. D. E. C. C. Corbridge, *The Structural Chemistry of Phosphorus* (Elsevier, Amsterdam, 1974).
38. R. R. Holmes, *Pentacoordinated Phosphorous Vol. I* (ACS Monograph 175, Washington, DC, 1980), vol. 1.
39. L. Pauling, in *The Nature of the Chemical Bond* (Cornell Univ. Press, Ithaca, NY, 1960) pp. 255–260.
40. A. S. Mildvan, *Proteins* **29**, 401 (1997).
41. G. Kemp, S. Trippett, *Tetrahedron Lett.* **48**, 4381 (1976).
42. F. H. Westheimer, *Acc. Chem. Res.* **1**, 70 (1968).
43. F. Ramirez, J. F. Marecek, *J. Am. Chem. Soc.* **101**, 1460 (1979).
44. J. R. Knowles, *Annu. Rev. Biochem.* **49**, 877 (1980).
45. Hydrogen bonds are made between the C(6)phosphate and the N118 side chain NH2, S116 side chain OH, K117 amide NH, the two R49 guanidinium NHs, Wat 231, Wat 48, Wat5, Wat129; hexose C(4)O and Wat129 and V47 amide NH; hexose C(3)O and Wat68; C(2)O and Wats68 and 29; and hexose C(5)O and S116 amide NH.
46. For this analysis, the model of the ligand β-G1,6-P was refined in a crystallography and nuclear magnetic resonance system with geometric constraints for normal tetrahedral hybridization at phosphorus during the initial stages of refinement of the 1.2 Å structure. The model of the ligand was docked into the active site by overlaying the hexose ring, C(6)phosphate, and C(1)phosphate phosphorus portion of the molecule with that of the pentavalent intermediate.
47. T. C. Bruice, F. C. Lightstone, *Acc. Chem. Res.* **32**, 127 (1999).
48. A. L. Morris, M. W. MacArthur, E. G. Hutchinson, J. M. Thornton, *Proteins* **12**, 345 (1992).
49. Supported by a grant from NIH (grant GM16099) (to K.N.A and D.D-.M). Use of the Advanced Photon Source was supported by the U.S. Department of Energy, Basic Energy Sciences, Office of Science, under contract no. W-31-109-Eng-38. Use of the BioCARS Sector 14 was supported by NIH, National Center for Research Resources, under grant number RR07707. Research was carried out (in part) at the HHMI beamline X4A at the National Synchrotron Light Source, Brookhaven National Laboratory. Coordinates have been deposited in the Protein Data Bank (accession codes 1O08 and 1O03, for G1P and G6P cocrystals, respectively). We thank W. W. Cleland, G. Petsko, D. Ringe, R. Holmes, and A. Mildvan for careful reading of the manuscript, and E. Peisach for his generous help with graphics.

Supporting Online Material
www.sciencemag.org/cgi/content/full/1082710/DC1
Materials and Methods
SOM Text
Figs. S1 to S4
Table S1
References

23 January 2003; accepted 25 February 2003
Published online 13 March 2003;
10.1126/science.1082710
Include this information when citing this paper.

Role of Mobile DNA in the Evolution of Vancomycin-Resistant *Enterococcus faecalis*

I. T. Paulsen,[1,2*] L. Banerjei,[1] G. S. A. Myers,[1] K. E. Nelson,[1] R. Seshadri,[1] T. D. Read,[1] D. E. Fouts,[1] J. A. Eisen,[1,2] S. R. Gill,[1] J. F. Heidelberg,[1] H. Tettelin,[1] R. J. Dodson,[1] L. Umayam,[1] L. Brinkac,[1] M. Beanan,[1] S. Daugherty,[1] R. T. DeBoy,[1] S. Durkin,[1] J. Kolonay,[1] R. Madupu,[1] W. Nelson,[1] J. Vamathevan,[1] B. Tran,[1] J. Upton,[1] T. Hansen,[1] J. Shetty,[1] H. Khouri,[1] T. Utterback,[1] D. Radune,[1] K. A. Ketchum,[1]† B. A. Dougherty,[1]‡ C. M. Fraser[1,3]

The complete genome sequence of *Enterococcus faecalis* V583, a vancomycin-resistant clinical isolate, revealed that more than a quarter of the genome consists of probable mobile or foreign DNA. One of the predicted mobile elements is a previously unknown *vanB* vancomycin-resistance conjugative transposon. Three plasmids were identified, including two pheromone-sensing conjugative plasmids, one encoding a previously undescribed pheromone inhibitor. The apparent propensity for the incorporation of mobile elements probably contributed to the rapid acquisition and dissemination of drug resistance in the enterococci.

The Gram-positive bacterium *Enterococcus faecalis* is a natural inhabitant of the mammalian gastrointestinal tract and is commonly found in soil, sewage, water, and food, frequently through fecal contamination (*1*). *E. faecalis* can withstand oxidative stress, desiccation, and extremes of temperature and pH, and it has high endogenous resistance to salinity, bile acids, detergents, and antimicrobials (*1*).

E. faecalis is an opportunistic pathogen that is a major cause of urinary tract infections, bacteremia, and infective endocarditis (*2*). The intrinsic resistance of *E. faecalis* to many antibiotics and its acquisition of resistance to other antimicrobial agents, particularly vancomycin, which is used to treat serious infections by drug-resistant Gram-positive pathogens, has led to the emergence of *E. faecalis* as a nosocomial pathogen that is refractory to most therapeutic options (*3*). Recent reports of the long-predicted emergence of vancomycin-resistant *Staphylococcus aureus* clinical isolates from transfer of enterococcal genes is a serious health care concern (*4*). Here we report the complete genome sequence of *E. faecalis* strain V583 (*5*), the first vancomycin-resistant clinical isolate reported in the United States (*6*). The genome sequence provides insight into the pathogenesis and biology of *E. faecalis*, the role of mobile elements in genome evolution, and the transfer of vancomycin resistance.

A total of 3337 predicted protein-encoding open reading frames (ORFs) were identified on the chromosome and three plasmids of *E. faecalis* V583 (Table 1; fig. S1) (*7*). Over a quarter of the *E. faecalis* V583 genome consists of mobile and/or exogenously acquired DNA, including seven probable integrated phage regions, 38 insertion elements (IS), multiple conjugative and composite

[1]The Institute for Genomic Research, 9712 Medical Center Drive, Rockville, MD 20850, USA. [2]Johns Hopkins University, Charles and 34th Streets, Baltimore, MD 21218, USA. [3]The George Washington University School of Medicine, Departments of Pharmacology and Microbiology and Tropical Medicine, 2300 Eye Street NW, Washington, DC 20037, USA.

*To whom correspondence should be addressed. E-mail: ipaulsen@tigr.org
†Present address: Celera Genomics, 45 West Gude Drive, Rockville, MD 20850, USA.
‡Present address: Bristol-Myers Squibb PRI, 5 Research Parkway, Wallingford, CT 06492, USA.